Caving 2022 - Y Potvin (ed.)

doi:10.36487/ACG_repo/2205_30

Seismic event location uncertainty in mining with reference to caving

IG Morkel *IGM Geotechnical, Australia*

J Wesseloo *Australian Centre for Geomechanics, The University of Western Australia, Australia*

Y Potvin *Australian Centre for Geomechanics, The University of Western Australia, Australia*

Abstract

The occurrence of seismicity in high stress underground environments is common and often leads to underground damage, affecting both the safety and profitability of a mine. To manage this risk, it is typical for a mine to install a seismic sensor array which is used to assess the seismic conditions around the excavations and monitor any changes to it.

Arguably, one of the most important seismic parameters to determine with any seismic network is the event locations. An accurate catalogue of event locations and times is a requirement for a good understanding of the seismic response to mining and the sources of seismicity. Unfortunately, the process of event location is challenging, and it is typical to have large errors on the location, especially in mining environments with large mine openings (e.g. caves).

In this paper, we discuss the results of a new method for estimating the event location uncertainties. We also discuss how this new method allows one to both improve the seismic sensor array to minimise location uncertainties, and how it allows geotechnical teams to consider the impact of inaccurate event locations in seismic interpretations.

Keywords: *mine seismicity, seismicity, location accuracy, quality, location error*

1 Introduction

The occurrence of seismicity in mining poses one of the biggest risks for mining companies, since large events can lead to considerable damage, which has an impact both on the finances, public profile, and safety record of the mining company. It is for this reason mines which have had historically damaging seismic events, invest in seismic systems to record seismicity at the mine.

The data from the seismic system can be used in multiple ways, but the most common uses are:

- Locating areas affected by large events to direct rescue efforts (Jager & Ryder 1999).
- Dynamic ground support design (Jager & Ryder 1999; Kaiser 1996).
- Calculation of seismic hazard trends (Morkel & Wesseloo 2017a; Wesseloo 2018).
- Used for in-depth seismic analyses (Gibowicz & Kijko 1994).
- Re-entry after blasting/firing or the occurrence of large events (Morkel & Rossi-Rivera 2017; Tierney & Morkel 2017).
- Calibration of numerical models (Jarufe et al. 2020).

A well-designed seismic system aims to ensure that the monitoring objectives from the geotechnical team are reached while maintaining the quality of the data. Examples of typical data quality artefacts and methods can be found in Morkel et al. (2015) and Morkel & Wesseloo (2017b).

Historically, system designs have mainly been based on two parameters. They are:

- **Mmin** – Also referred to as the magnitude of completeness. A parameter which describes the smallest magnitude which can reliably be recorded for a volume or a specific point in the mine based on the seismic network layout. This parameter depends on the minimum sensors used for processing, as well as a PPV-distance equation (which describes wave attenuation). The preference is a calibrated PPV-distance equation, but when this is not possible, theoretical options are available (e.g. Kaiser & Maloney 1997; Potvin & Wesseloo 2013; Wesseloo 2018).
- **Estimated location error** – A parameter describing the expected location error at a specific point in the mine, based on the size of the event, the seismic network layout, the minimum sensors used in processing, and the PPV-distance relationship. This parameter is done for larger magnitudes (ML >0).

Several case studies are available describing the system design process using these parameters. These include empirical methods (e.g. Wesseloo 2011) and numerical (e.g. Nyström & Mozaffari 2017). These studies are adequate for most mines, where the following conditions apply:

- It is assumed that excavations/voids are not large enough to adversely affect the travel path of event-sensor rays.
- The seismic system being designed is not overly planar, leading to large errors perpendicular to the sensor plane.

Unfortunately, for caving mining methods, at least one of these conditions does not apply. Either the ray paths between events and sensors are adversely affected by the scale of the void; or the sensors, although installed in a 3D setup, have the properties of a planar network. This is because of the large void created by the cave leading a circular plane around the cave.

Therefore, we propose an alternative method for determining location errors, which, although specifically designed for mines with large excavations, has a practical use in all other mining setups.

2 Event location uncertainty

In this section, we investigate the impact of seismic network sensor layouts on the location uncertainty of events. This is done by investigating typical network location artefacts and then determining the ability of the new method (see Section 3 for the IGM estimated location uncertainty metric) to replicate them. Further to this, we also want to ensure that the new method can reproduce some properties of the old method, specifically the scale of location error.

We describe the IGM metric as an estimated location uncertainty and not as an estimated location error. This is because location error, as is used conventionally (e.g. Wesseloo 2011; Nyström & Mozaffari 2017), does not describe the error as an explicit result of the uncertainty in calculation parameters (e.g. velocity and arrival times). Where with the IGM metric, this is the case.

An example of a plot of the estimated location error is shown in Figure 1 (from Zvarivadza et al. 2017). The location error for this plot is estimated for an event magnitude of zero. From the plot, the smallest estimated location errors are situated in the centre of the network, with errors less than 10 m, gradually increasing as the points are further away from the installed sensors. Estimated location errors in the outer edges of the network are as large as 50–100 m. An increase in sensor density leads to an increase in estimated event location accuracy. The plot only indicates the scalar unit of the estimated location error and does not describe the directionality of the error.

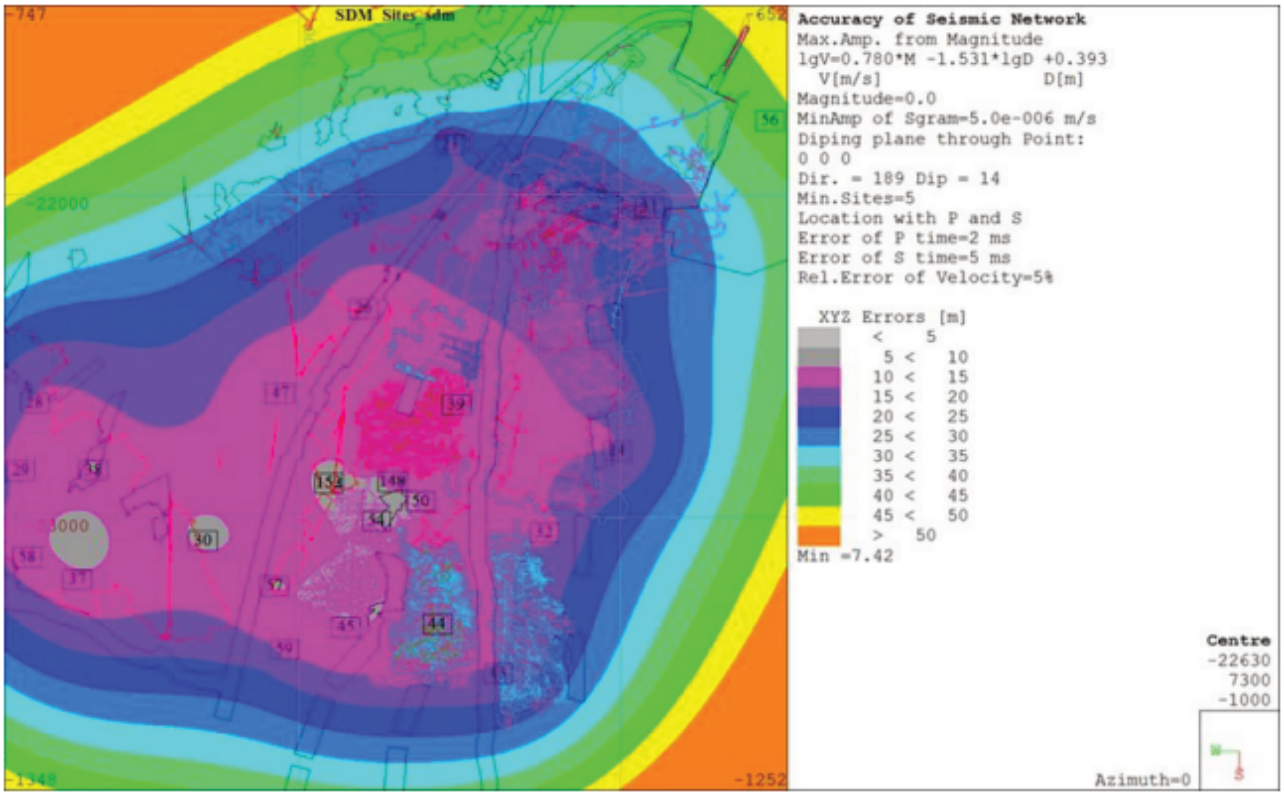

Figure 1 Typical location error plot for a mine (from Zvarivadza et al. 2017)

2.1 Location artefacts

We have noticed that some practitioners and consultants do not have a good understanding of typical event location artefacts. Because of this, some interpretations of seismic behaviour and likely seismic sources are misguided. An example of this is the interpretation of mirrored sources as hanging wall/footwall events when those events are misslocated because of a mirroring effect (explained below).

These artefacts result from both network layout limitations and the inability of the location algorithm to confine the location of events in a certain area to a single unique XYZ. Some of the location error artefact that occurs in mine seismicity databases are illustrated in this section below (with three case studies).

The first example of location artefacts is the occurrence of mirrored events in some seismic databases (see Figure 2). Mirrored events are events which have, because of the planarity of the seismic network, not a well-defined event location. The events are therefore located either ‘above’ or ‘below’ the plane, a ‘mirror’ of the true location. Some service providers have introduced a directional wave component to limit the occurrence of mirroring. From our experience this has, however, seen limited success, and mirroring in databases is still common.

The second common location artefact seen in databases is the occurrence of ‘donut’ shapes (Figure 3). These events are all located in the same area (production driven in this case) but due to the inability of the location algorithm to confine the location accurately, events are spread in a donut shape. These artefacts occur when sensors are located along a straight (cylindrical) line. From our experience, it is not typical to see this type of artefact for larger events but is common for events triggering five sensors or less.

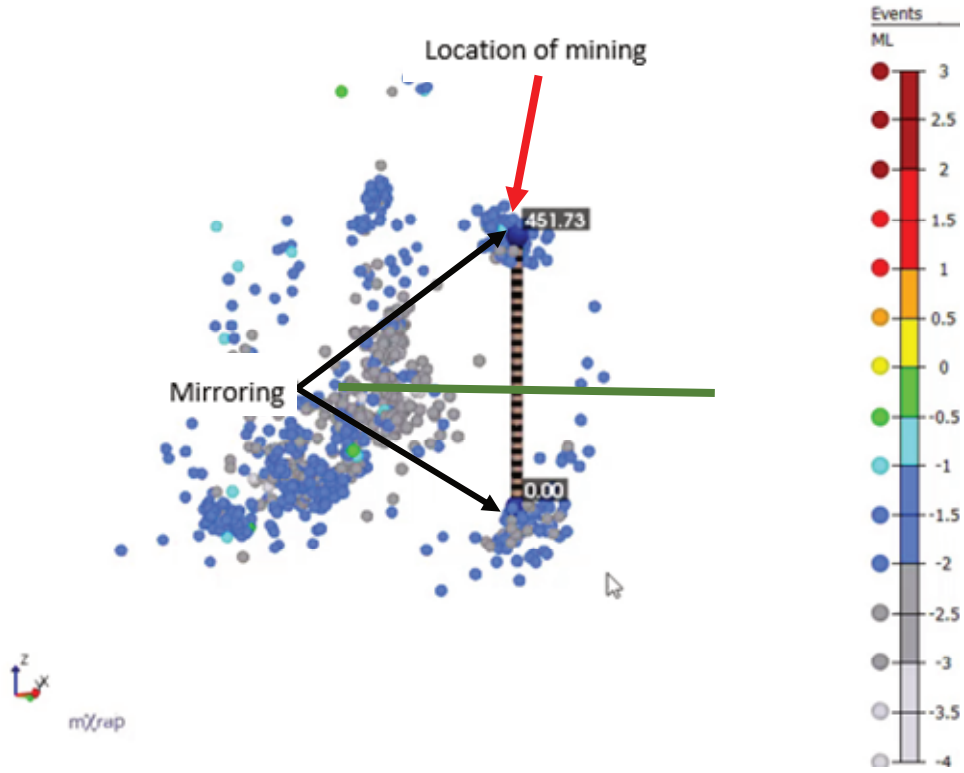

Figure 2 **View along a plane of sensors for Mine A. The green line indicates the sensor's plane, and the spheres indicate the recorded events coloured according to the magnitude. The black arrow indicates the events which are mirrored, and the red arrow indicates the area where mining (production) is taking place**

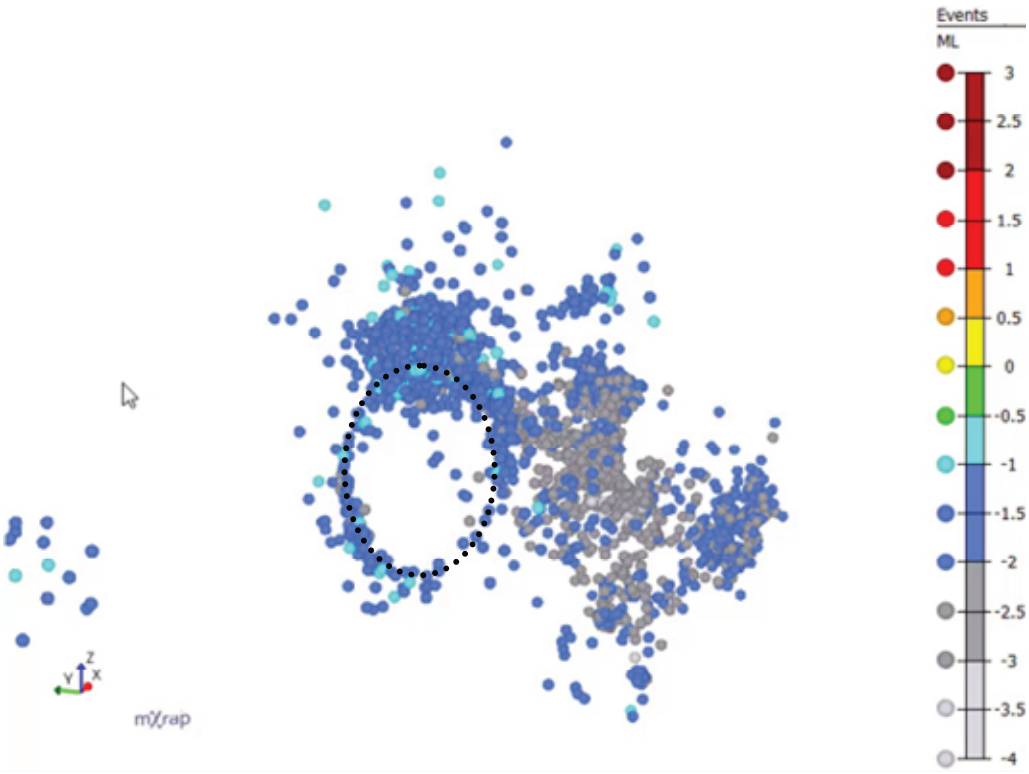

Figure 3 **'Donut' shaped location artefact (indicated by the black dashed circle) seen for a typical mine database. The seismic events are indicated by the spheres, coloured according to magnitude**

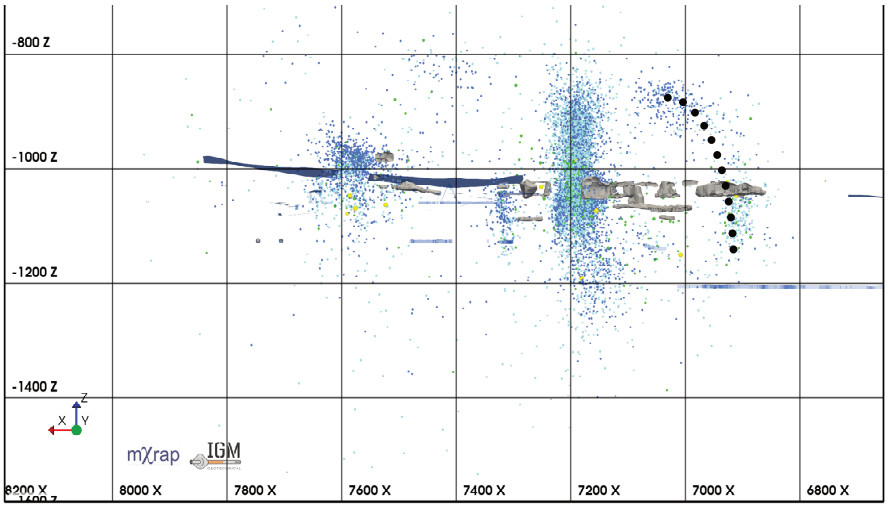

Figure 4 'Banana' shaped location artefact (indicated by the black dashed circle) seen for a typical mine database. The seismic events are indicated by the spheres, coloured according to magnitude

The final artefact is seen for most seismic networks in areas on the peripheral of the network. These artefacts are referred to as 'banana-shaped' (Figure 4), and they are observed in all mines, where sensors do not cover the extent of mining (sensors are not installed beyond active mining areas). Events are located outside of the seismic network. The longest axis of these banana-shaped artefacts is in the direction perpendicular to the plane best describing the sensor locations.

2.2 Probabilistic analysis

Current methods cannot replicate the location artefacts which were described in the section above. The aim of this paper is to describe the expected location uncertainty in such a way that we can replicate the location artefacts. Therefore, it is required to describe the parameters leading to the uncertainty in the event location.

A first approach to understand the uncertainty in event location is done through a Monte Carlo simulation. In the Monte Carlo approach, we investigate the impact of the event S-wave and P-wave velocities and picks on the event location. The result is a unique event location for each combination of the parameters, resulting in a cloud of viable locations.

For the Monte Carlo simulation, the P- and S-wave picks and velocities are altered according to their uncertainties, and an event location is calculated for each set of combinations. The distributions for the picks and the velocities are assumed to be normally distributed. For the examples shown below, 10,000 samples are produced, which is then plotted.

To determine the uncertainty in velocity, the slope of the best fit line of the sensor distance versus travel time plot is done for each event in the database. The best fit P- and S-velocities are then evaluated to determine the uncertainty in the velocities. Figure 5 a histogram of the S-wave and P-wave velocities for all events in the database. The mean P-wave and S-wave velocities of 6,435 and 3,655 m/s respectively closely corresponded with the velocities used by the service provider for seismic processing at this mine. Standard deviations for the P-wave and S-wave velocities of 550 and 232 m/s respectively were determined. Velocity distributions (based on the mean and standard deviations values) were used in the Monte Carlo analysis.

Further to the uncertainty of the velocities, we also investigated considered the uncertainties in the choice of the P- and S-picks of the data. For the uncertainty in picking, an assumed standard deviation was decided on based on previous experience. A standard deviation of 1 microseconds was assumed for both the P- and S-pick uncertainty.

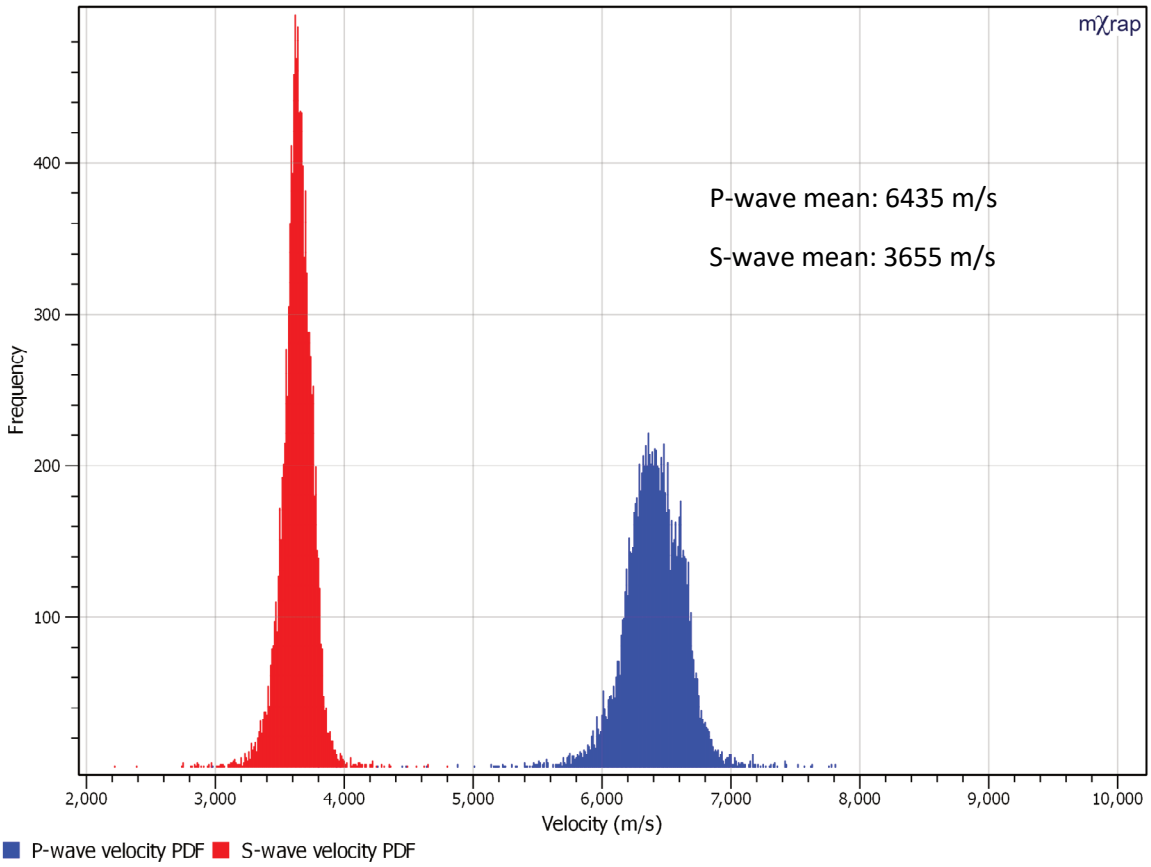

Figure 5 Velocity distributions for Mine A with average values for the P- and S-waves. The red distribution is for the S-wave velocities, and the blue distribution is for the P-wave velocities

The Monte Carlo results for three different events are shown in Figure 6. These events were specifically selected to investigate if it is possible to produce the three artefacts discussed before with a statistical method.

Figure 6 top left, an example of mirroring seen in the database due to the planarity of the sensors used. There is a high likelihood an event located in one cloud could be located in the opposite cloud because of the inability of the sensor layout to confine the locations to a single area.

Figure 6 top right an example of a ‘donut’ shaped artefact for an event at Mine A. The cloud produced is for an event which triggered four sensors.

Figure 6 bottom left, shows an example of a ‘banana’ shaped artefact seen at Mine A. The Monte Carlo cloud is for a larger event (ML ~0) occurring on the proximity of the network. It is clear the location of the event does not ensure a 3D coverage and therefore the banana shape occurs.

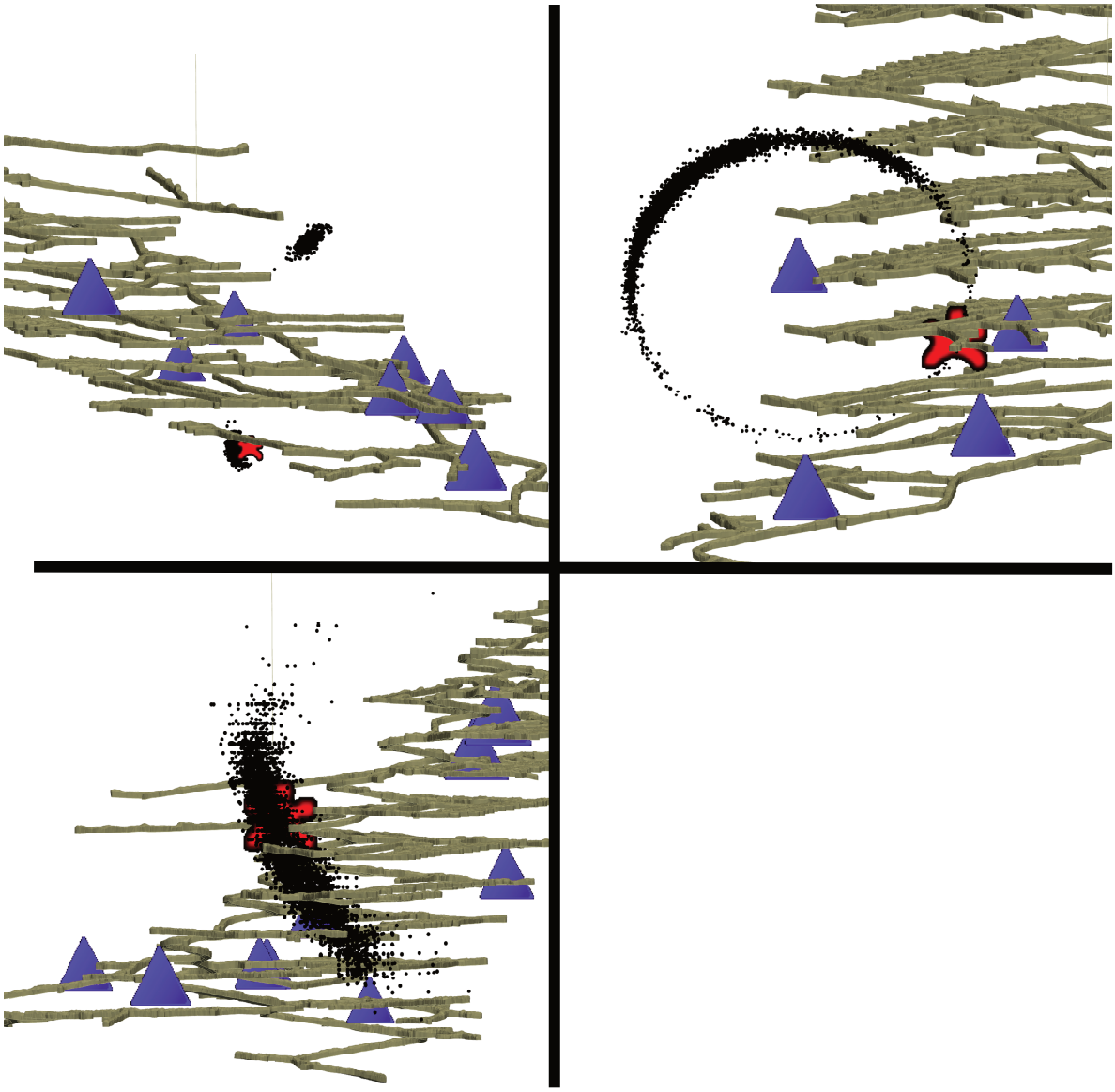

Figure 6 (top left) Example of mirroring seen from the Monte Carlo results (top right) Example of a 'donut' shape seen from the Monte Carlo results (bottom left) Example of a 'banana' shape seen from the Monte Carlo results. The triangles indicate triggered sensors, while the red star indicates the location of the event in the database

The described Monte Carlo process effectively replicate the location artefacts seen for a typical mine seismic database. It is also important that the method also replicate the decreased uncertainty with increased sensor density. The results of such an analysis are shown in Figure 7**.** In Figure 7, the left-hand example is for an ML -1.4 event outside of the seismic network, while the example on the right is for an ML -1.4 event inside the densest part of the network. It can be seen that the spread of the location cloud from the Monte Carlo analysis is much larger (~150 m) for the event outside of the network (Figure 7 left), while this spread is only ~50 m for the same sized event within the network (Figure 7 right). This is similar to what was seen for the location error in Figure 1, which shows that this probabilistic method can reproduce those previous results.

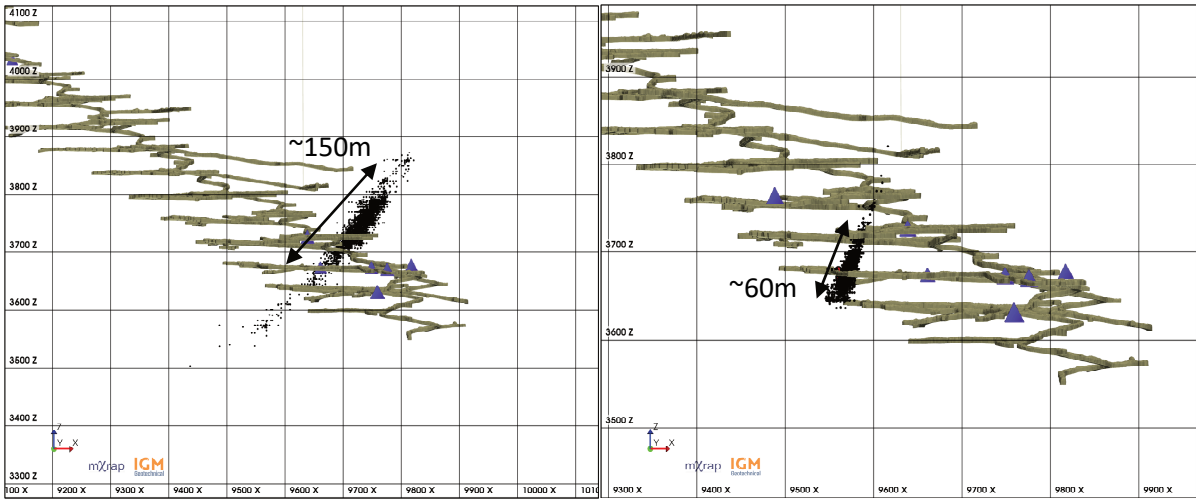

Figure 7 (left) Monte Carlo cloud for ML -1.4 event outside the seismic system bounds; (right) Monte Carlo cloud for ML -1.4 event within the seismic system bounds

In this section, we could show that with a simple Monte Carlo analysis, we can reproduce all the artefacts identified for a typical database. This technique therefore can capture the effect of the major system contributors to event location inaccuracies.

This technique, however, needs reasonable input parameter distributions (usually based on historical data), and a P- and S-velocity and picks are required in order to run this type of analysis. However, when doing a system design, these parameters are not available, and therefore this method is not possible for system design use.

3 IGM location uncertainty metric

In this section, we present the IGM location uncertainty metric developed at IGM Geotechnical. The metric provides a simplified and fast approach to model the location artefacts seen for a typical mine seismic database model of the system in a similar way to the Monte Carlo approach presented in the previous section. The input to the IGM location uncertainty metric is limited to a strong ground motion relationship and sensor locations.

The preference is that the strong ground motion relationship is calibrated to site data to ensure; the algorithm used in determining which sensors are triggered is accurate. Further to this, a historical triggering PPV for each sensor type is also required.

In the following sections, we compare the results from the IGM metric to those produced by the Monte Carlo analyses. Finally, we discuss a case study to illustrate the usefulness of this new method.

3.1 Location artefact results

All three types of artefacts discussed previously are investigated in this section. The results are based on the database from Mine B. In Figure 8 are similar artefacts to what was described before (Figure 6), but also included is the surfaces from the IGM metric (similar to before the black dots are the results from the Monte Carlo method). The IGM metric in these cases use the same sensors which were triggered for the specific event evaluated. The IGM metric surfaces are coloured according to uncertainty, with warm colours indicating the areas with the highest event probability.

It can be shown that the IGM metric can replicate the Monte Carlo results for these artefacts. Figure 8 presents the IGM metric surfaces for the three artefacts discussed before. Both the Monte Carlo points, and triggered sensors are indicated for each example.

The surface contours for the IGM metric are continuous and generate very low probabilities in some areas (this is because it is a based on an algorithm), while the results from the Monte Carlo method are discrete. Therefore, locations based on the Monte Carlo method are located in the high probability zones of the IGM metric surface; if more Monte Carlo runs are done, the results will fill out the low probability areas. The metric can reproduce these artefacts and is ideal for system design as it allows users to remove or add sensors to the system and determine their impact on the expected location uncertainty.

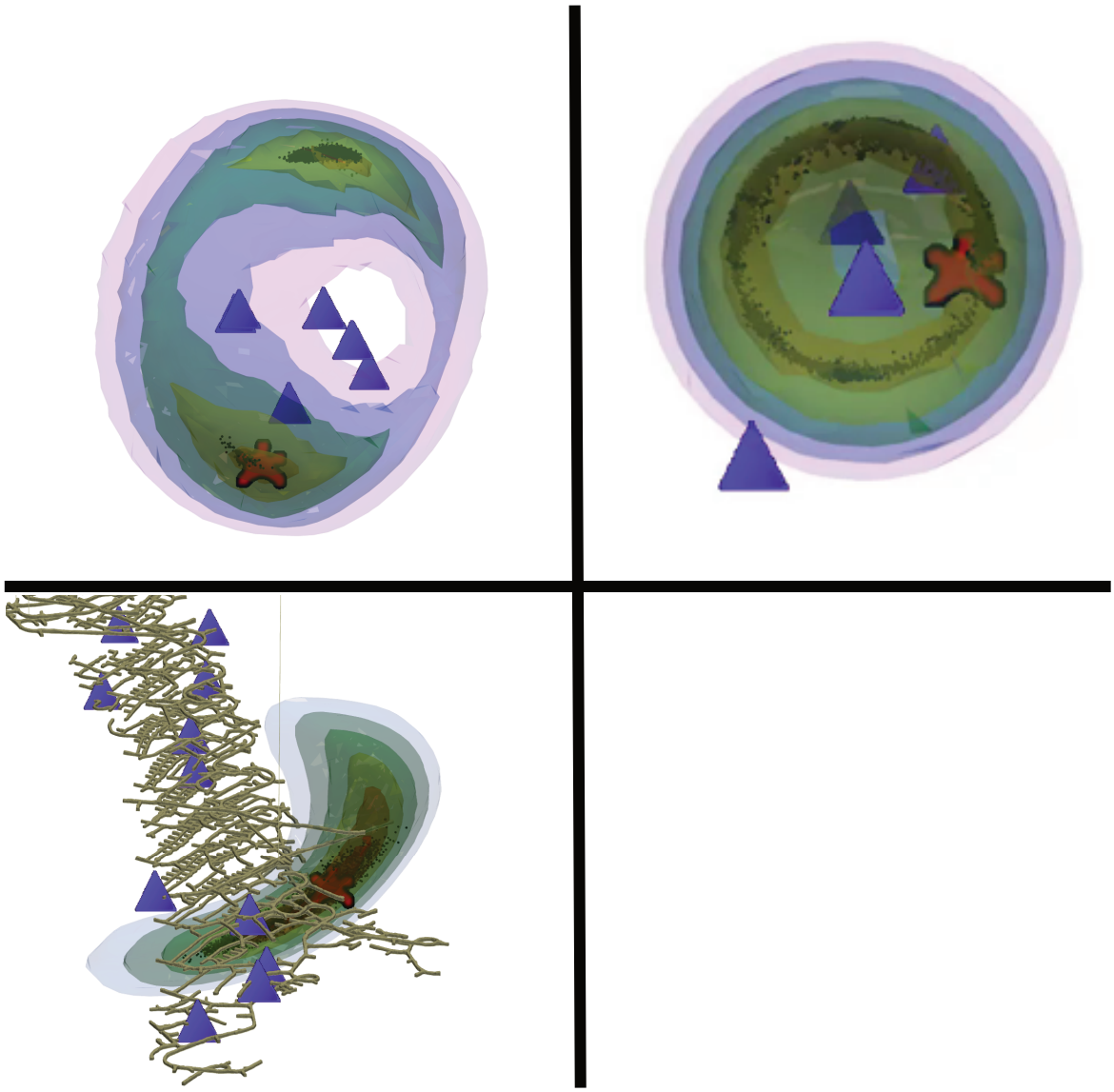

Figure 8 The IGM metric results for the three different artefacts discussed before. The triangles indicate the triggered sensors, the block dots indicate the Monte Carlo points, and the coloured surfaces indicate the IGM metric results (warm colours indicate high event location probability). (top left) Mirroring artefact (top right) 'donut' shaped artefact (bottom left) 'banana' shaped artefact

3.2 System maintenance and data interpretation

The IGM metric provides a method to quantify the system limitations and associated uncertainty in event locations and providing a context for data interpretations. An example of this is the association of events with geological structures (e.g. dykes). Many techniques rely primarily on the event location to determine the statistical properties of a structure. Therefore, the ability to investigate if the location of events along a structure can be assumed to be reasonable is useful. If the error is so large that the event locations are not usefully confined to that surface, then the results from the analysis cannot be trusted.

To evaluate the uncertainty along a plane of points, an uncertainty vector is calculated. The uncertainty vector is the vector which is calculated along the axis with the largest IGM uncertainty. An example of such event uncertainty vectors is shown in Figure 9.

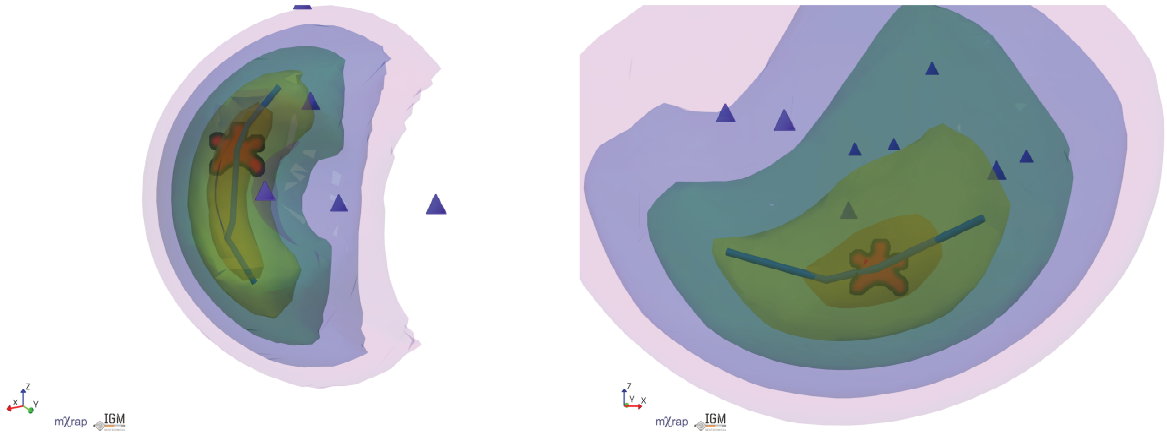

Figure 9 Theoretical location uncertainty surfaces for two seismic events. For each event an uncertainty vector (blue lines) is calculated which describes the largest dimensional error for that surface. The blue triangles indicate the sensor locations used

To determine the usefulness of calculating an uncertainty vector, an example of a typical mine with several structures was investigated. During the investigation, two structures were specifically considered, the first structure cuts almost perpendicularly across the orebody (Figure 10 top), while the second structure runs almost parallel with the orebody (Figure 10 bottom). It is clear from the vectors in Figure 10, that event locations are much better confined to the structure running across the orebody than for a structure running along the orebody.

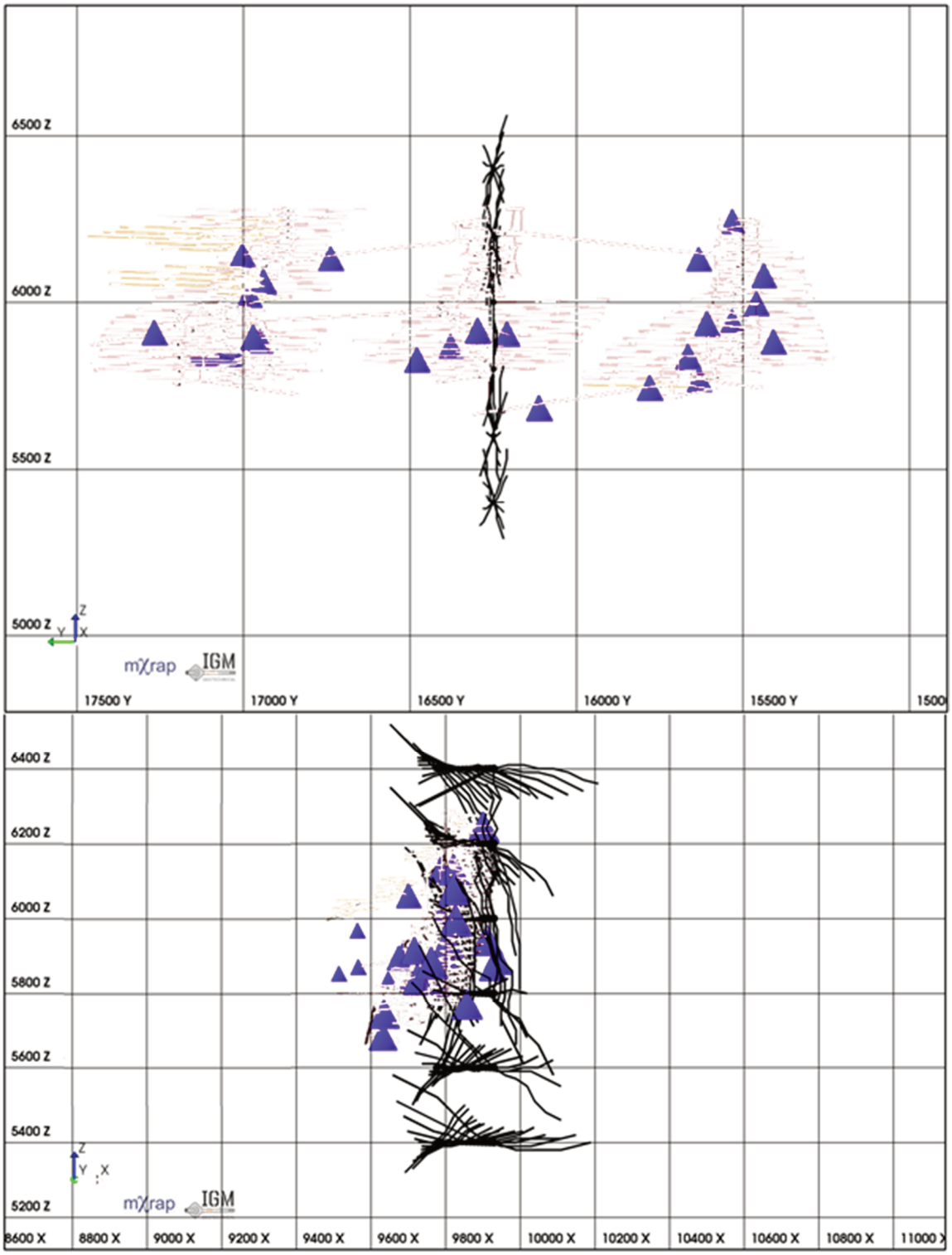

Figure 10 Uncertainty vectors for two structures within a mining network. (top) Uncertainty vectors for a structure running through the orebody; (bottom) Uncertainty vectors for a structure running along the orebody. Triangles indicate sensors in the network. The vectors are based on an events size of ML 0

The results which were discussed in this section assumed a homogenous rock mass where the impact of voids is negligible on the event-sensor ray paths (since it is assumed to be straight).

4 Ray-tracing

The IGM metric is not defined in terms of location algorithm, and therefore the metric can be calculated for ray paths. This will be illustrated in the example below, since the ability to use ray-tracing algorithms is critical to ensure accurate locations in caving. We discuss the location uncertainty for an event occurring in the hanging wall of a sublevel cave, and the impact of the void on the location uncertainty of such events. This is done by calculating the IGM metric for ray-tracing simulation code. In the example, we will compare the results from the straight-line code and the ray-tracing code to illustrate the differences, and then discuss this using a case study.

An example is chosen where an event occurs in the hanging wall of a sublevel cave, with all the seismic sensors located in the footwall. We simulate two scenarios; the first is an event centrally located in the hanging wall of a sublevel cave, while the second scenario is for an event on the edge of a cave (typically where production takes place). For each scenario, we investigate the IGM metric uncertainty volumes (similar to Figure 8) and consider the impact of calculating event locations assuming both ray-tracing and straight paths. The setup of the simulations is for a sublevel cave where the location of the event is recorded by four sensors installed at different depths.

4.1 Scenario 1: Event on the edge of the cave

In the first scenario, an event on the edge of the cave is simulated. The results for the simulation are shown in Figure 11. Figure 11 left the results assuming straight paths, and Figure 11 right the results assuming ray-tracing. In both figures, the dark blue squares indicate the cave void, the numbers indicate the location of the seismic sensors and the red star the simulated event location. A section (on the event elevation) for the IGM metric uncertainty is indicated by the coloured surface. Red colours indicating locations with the highest event probability.

The results from the simulation reveal that the event in both cases is located within the IGM metric curves (coloured squares). Further to this, the shape and size of the uncertainty area is similar for both the straight-path and ray-tracing examples. This is expected, since events on the edge of the cave will have event-sensor paths which have been minimally affected by the cave void.

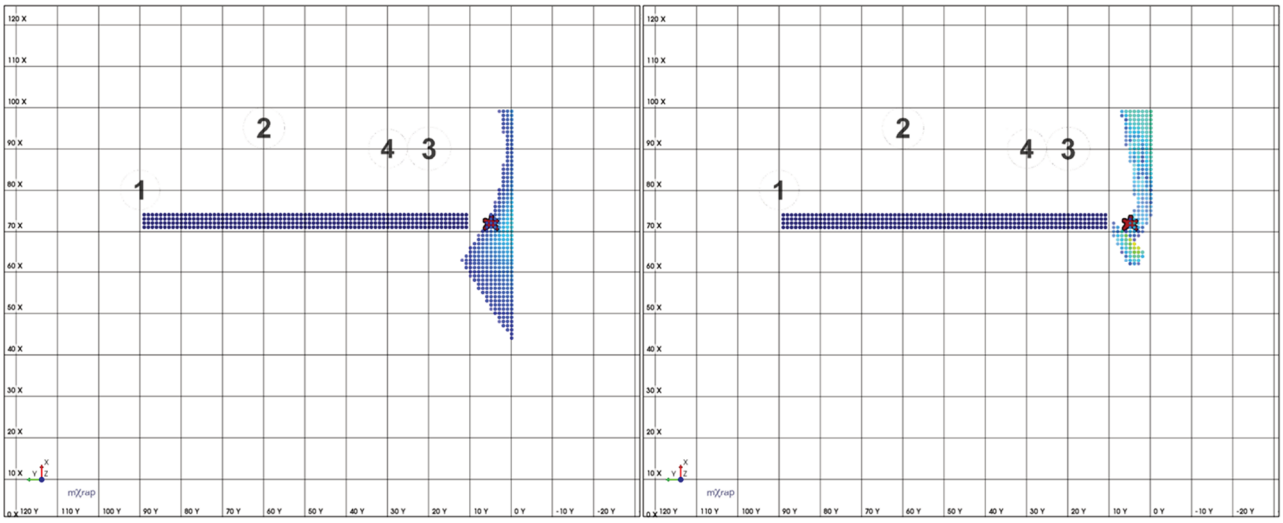

Figure 11 IGM metric results for an event simulated on the edge of a sublevel cave (red star). (left) The IGM metric results assuming straight paths; (right) IGM metric results assuming ray-tracing. The cave void is indicated by the dark blue squares. The numbers indicate the sensor locations. The coloured squares are a section of the IGM event uncertainty volume

4.2 Scenario 2Event in the hanging wall

In the second scenario, the occurrence of an event in the centre of the cave's hanging wall is simulated. The results for this scenario are shown in Figure 12. Similar to before, the sensors used are indicated by the numbers, the simulated event location is indicated by the red star, and the cave void by the dark blue squares. The coloured surface is a section (on the event elevation) of the IGM metric assuming straight paths (Figure 12 left) and assuming ray paths (Figure 12 right).

Events in the hanging wall of the cave will have event-sensor paths which are affected considerably by the cave void. It is clear from the results that, when considering ray-tracing, the event location (Figure 12 right) is within the IGM metric volume. In contrast, when assuming straight paths (Figure 12 left) the IGM metric is located well into the hanging wall far removed from the simulated event location. This would mean that when an event occurs in the hanging wall and is located assuming straight event-sensor paths, those events will be wrongly located deep into the hanging wall.

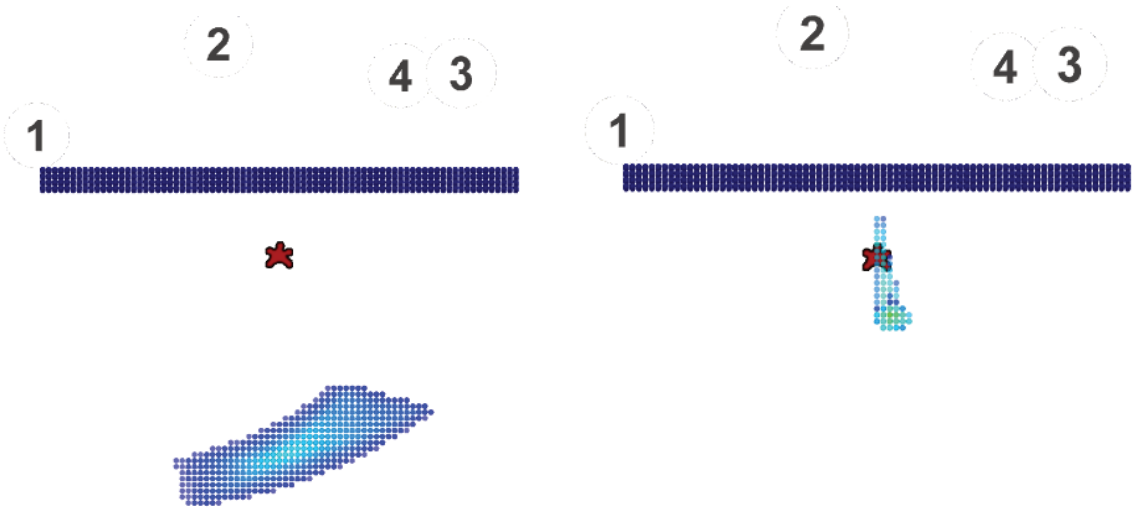

Figure 12 IGM metric results for an event simulated in the centre of a sublevel cave's hanging wall (red star). (left) The IGM metric results assuming straight paths; (right) IGM metric results assuming ray-tracing. The cave void is indicated by the dark blue squares. The numbers indicate the sensor locations. The coloured squares are a section of the IGM event uncertainty volume

Consider a section from Mine C, a sublevel caving mine (Figure 13). The cave void is indicated by pink surfaces, while the events are indicated by spheres coloured according to magnitude. In this simple example events in the hanging wall are located deep into the rock mass, and spread out across the caving front.

Based on the simulation in Figure 12, we propose that those events are most likely much closer to the caving void, and that the spread across the caving front is because of the uncertainty in the locations, and is not a property of the rock mass response. When applying ray-tracing code to the event database, the events will move closer to the cave and could likely form linear lines along structures or the caving abutment where cave production is taking place.

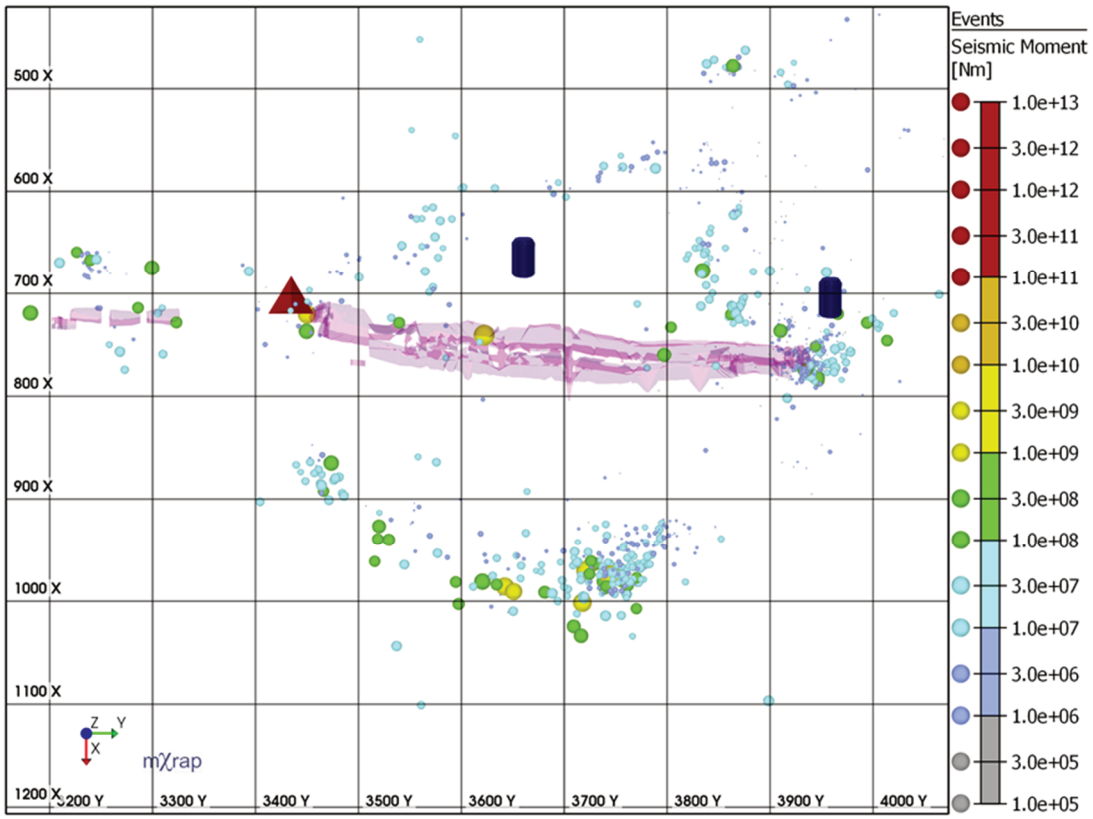

Figure 13 A section through a typical block caving mine. Mined-out areas are indicated with the pink surfaces. Events are indicated with the coloured spheres, larger events are indicated with warmer colours. Seismic sensors are indicated with the cylinders and triangles

The next step of this project is to reprocess events for a block cave similar to the example in Figure 13, and indicate the usefulness of the IGM metric for such an analyses. The reprocessing attempt will adapt a ray-tracing component, but we will also investigate (using the new metric) the impact of having sensors installed in the hanging wall.

5 Conclusion

The IGM metric improves on current estimated location error techniques (discussed in Section 1) by adding additional spatial dimensions to estimated location error. This allows for location errors to be plotted as vectors or uncertainty volumes. Practitioners can plot the event location uncertainty on points on a section or along a structure, and use the results to determine confidence in spatial analysis results.

The IGM location uncertainty metric can replicate commonly seen location artefacts in databases with accuracy. This allows for more in-depth system designs that eliminate these artefacts and gives confidence in event location and therefore sources of seismicity.

Due to its simplicity and the fact that it relies on limited, readily available input, the IGM location location uncertainty metric provides an effective tool for both managing artefacts in the system, but also would allow to analyse the location uncertainty vectors to understand the limitations of the current system.

Further to this, the metric is also not reliant on explicit assumptions in event locations algorithms (e.g. straight paths versus ray-tracing). This allows practitioners to use this metric in mining methods which are more complex than most mines (e.g. sublevel and block caving) and generate accurate uncertainty volumes.

Acknowledgement

The authors acknowledge the mXrap team; the app was designed using their software (Harris & Wesseloo 2015).

References

Gibowicz, SJ & Kijko, A 1994, *An Introduction to Mining seismology*, 1st edn, Academic Press, Cambridge, p. 404.

Harris, PC & Wesseloo, J 2015, *mXrap*, version 5, computer software, The Australian Centre for Geomechanics, Perth, www.mXrap.com

Jager, A & Ryder, J 1999, *A Handbook on Rock Engineering Practice for Tubular Hard Rock Mines*, Safety in Mines Research Advisory Committee, Johannesburg.

Jarufe, J, Wesseloo, J, Potvin, Y & Dhanér, C 2020, 'Numerical modelling calculation of probabilistic seismic hazard in cave mining', in R Castro, F Báez & K Suzuki (eds), *MassMin 2020: Proceedings of the Eighth International Conference & Exhibition on Mass Mining*, University of Chile, Santiago, pp. 1225–1234, https://doi.org/10.36487/ACG_repo/2063_90

Kaiser, PK 1996, *Canadian Rockburst Support Handbook*, prepared for Sponsors of the Canadian Rockburst Research, Geomechanics Research Centre.

Kaiser, PK & Maloney, SM 1997, 'Scaling laws for the design of rock support', *Seismicity Associated with Mines, Reservoirs and Fluid Injections*, Springer, Berlin, pp. 415–434.

Morkel, IG & Rossi-Rivera, P 2017, 'The implementation and quantification of the Vallejos and McKinnon re-entry methodology', in J Wesseloo (ed.), *Deep Mining 2017: Proceedings of the Eighth International Conference on Deep and High Stress Mining*, Australian Centre for Geomechanics, Perth, pp. 173–181, https://doi.org/10.36487/ACG_rep/1704_10_Morkel

Morkel, IG & Wesseloo, J 2017a, 'The effect of sensor frequency range on the estimation of the current hazard state', in Submitted (ed.), 9th International Symposium on Rockbursts and Seismicity in Mines, 15-17 November 2017 2017a, Santiago, Chile.

Morkel, IG & Wesseloo, J 2017b, 'A technique to determine systematic shifts in microseismic databases', in J Wesseloo (ed.), Proceedings of the Eighth International Conference on Deep and High Stress Mining, 28-30 March 2017b, Perth, Australian Centre for Geomechanics, pp. 105-116.

Morkel, IG, Wesseloo, J & Harris, P 2015, 'Highlighting and quantifying seismic data quality concerns', in PM Dight (ed.), *FMGM 2015: Proceedings of the Ninth Symposium on Field Measurements in Geomechanics*, Australian Centre for Geomechanics, Perth, pp. 539–549, https://doi.org/10.36487/ACG_rep/1508_37_Morkel

Nyström, A & Mozaffari, S 2017, 'Evaluation of microseismic array performances: case study of', *RaSim9: Proceedings of the 9th Symposium on Rockbursts and Seismicity in Mines*.

Potvin, Y & Wesseloo, J 2013, 'Towards an understanding of dynamic demand on ground support', *Journal of the Southern African Institute of Mining and Metallurgy*, vol. 113, pp. 913–922.

Tierney, SR & Morkel, IG 2017, 'The optimisation and comparison of re-entry assessment methodologies for use in seismically active mines', in J Wesseloo (ed.), *Deep Mining 2017: Proceedings of the Eighth International Conference on Deep and High Stress Mining*, Australian Centre for Geomechanics, Perth, pp. 183-196, https://doi.org/10.36487/ACG_rep/1704_11_Tierney

Wesseloo, J 2011, 'Empirical methods for assessment of seismic system sensitivity', *Mining Technology*, vol. 120, no. 2, pp. 105–111.

Wesseloo, J 2018, 'The spatial assessment of the current seismic hazard state for hard rock underground mines', *Rock Mechanics and Rock Engineering*, vol. 51, no. 6, pp. 1–24.

Zvarivadza, T, Sengani, F & Adoko, A 2017, 'In-stope pillar scaling and fracturing in Southern African deep level gold mines', *Proceedings of the 26th International Symposium on Mine Planning and Equipment Selection*, Luleå University of Technology, Luleå, pp. 29–31.